J Mater Sci (2008) 43:3452–3458
DOI 10.1007/s10853-008-2517-1

NANOSMAT 2007 - INTERNATIONAL CONFERENCE ON SURFACES, COATINGS AND NANOSTRUCTURED MATERIALS

Thermal stability and oxidation behavior of Al-containing nanocrystalline powders produced by cryomilling

A. Almathami · E. Elhachmi · M. Brochu

Received: 7 July 2007 / Accepted: 30 January 2008 / Published online: 21 February 2008

Abstract Al-containing nanostructured coatings provide excellent protection from high temperature corrosion. Aluminum oxide scales generally provide better oxidation resistance and yield lower oxidation rates than other oxide scale compositions. In this study, nanocrystalline 316L stainless steel containing 6 wt.% Al was synthesized using cryogenic milling (cryomilling). Complete alloying was obtained after 32 h of milling and the average grain size was found to be 7 nm. High temperature thermal stability and oxidation kinetics of the alloyed powders were examined. The powder demonstrated good grain growth stability at 500 °C, at which point, the powders had been heat treated for 120 h and the average grain size was found to be 11.4 nm. The oxidation kinetics of the powder were studied for 48 h at 500, 800, and 1,000 °C, respectively. For comparison, conventional 316LSS powder was also tested. Nanocrystalline 316LSS-6 wt.% Al showed lower weight gain than the conventional 316LSS powders. During the oxidation of nanocrystalline 316LSS-6 wt. % Al at 500 °C, protective aluminum oxide scale formed at the surface. At 800 °C and 1,000 °C, most of the nanocrystalline 316LSS-6 wt.% Al particles showed completed outer aluminum oxide scale. However, at 800 and 1,000 °C, some particles showed growth of chromium oxide scale underneath the aluminum oxide scale. In those samples, Al depletion was also observed due to a non-homogenous distribution of Al during cryomilling. The activation energy of the oxidation reaction was calculated and was found to be affected by the enhancement of the grain boundary diffusion in nanostructured particles.

A. Almathami · M. Brochu (✉)
Department of Mining and Materials Engineering,
McGill University, Montreal, Canada
e-mail: mathieu.brochu@mcgill.ca

E. Elhachmi
Materials Technology Laboratory, Natural Resources Canada,
Ottawa, Canada

Introduction

Oxidation is the most important high temperature corrosion reaction in furnaces and boilers. The oxides of iron, nickel, and cobalt, which are the alloy bases for most of the engineering alloys, have significantly lower thermodynamic stability compared to the oxides of some of the solutes such as aluminum, chromium, and magnesium. Traditionally, ferritic steels containing chromium (e.g., 5%Cr–0.5Mo, 7%Cr–0.5Mo, and 9Cr–1Mo) are used in the construction of tube bundles for boilers and furnaces due to their considerably reduced cost and high thermal conductivity [1]. The effect of the observed corrosion rates on the service life of tube bundles has been estimated for 9% chromium steel by Quadakkers et al. [2]. Based on the data determined by Quadakkers et al., the effects of oxidation on the service life of tube bundles cannot be neglected when examining wall thickness composed of 9% chromium below about 6 mm.

Aluminum oxide scales generally provide better oxidation resistance and yield lower oxidation rates than other oxides such as chromium oxide scale. Stainless steels (specifically the 300 series of Stainless Steel (SS)) are used widely for high temperature corrosion applications in furnaces and boilers. Significant developments have been made in an effort to partially replace chromium with aluminum in austenitic 300 series stainless steels to change the formation of oxide scale from chromium oxide scale to aluminum oxide scale during oxidation [3]. The oxidation

behavior of these alloys shows superior oxidation resistance in the temperature range between 800 and 1,100 °C and was demonstrated to be moderately resistant to oxidation up to 1,300 °C. The excellent oxidation resistance is attributed to the formation of continuous aluminum oxide film, Al_2O_3 [3].

The formation of aluminum oxide should be continuous, compact, and adherent to provide the maximum corrosion protection. The concentration of aluminum as a solute in the alloy should be above the critical concentration necessary to establish a complete pore-free surface layer of aluminum oxide. In practice, the higher aluminum concentration is necessary for the closely spaced precipitates to coalesce to form the healing layer [4, 5].

Nanostructured materials have been found to possess a high resistance for high temperature oxidation. Nanostructured coatings also promote the selective formation of protective oxidation scales due to the high density of grain boundaries, which provide fast diffusion paths [6]. In addition, scale adhesion and spallation resistance are improved by stress release and the micro-pegging effect [6]. In nanostructured alloys, the aluminum content required to form a complete protective oxide scale can be substantially reduced. Work performed by Gao and Zhengwei showed that for nanocrystalline Ni–20Cr–Al containing $\sim$2 wt.% of aluminum a complete α-Al_2O_3 scale could be developed at 1000 °C in air. This concentration is only one-third of the required aluminum content in the Ni–20Cr–Al alloy with normal grain size [6].

The present study was conducted to explore the oxidation behavior of nanocrystalline 316LSS-6 wt.% Al. The material was produced by cryomilling, a process in which powders are mechanically milled in slurry composed of milling balls and a cryogenic liquid [7]. The resulting powders were investigated as potential coating feedstock for the tube bundles of boilers and furnaces used in industrial applications.

Experimental

SS316L powders (16%Cr, 17.7%Ni, 2.2%Mo, 0.13%Mn, 0.75%Si, 0.01%C, balance Fe) from North American Hoganas were blended with 6 wt.% elemental Al powder from Atlantic Equipment Engineers. The cryomilling process (Union Process attritor) was used to alloy the powders and to refine the grains to nanometer scale. The apparatus included a thermocouple that was used to monitor the temperature in the attritor and to ensure a constant level of liquid nitrogen. Evaporated liquid nitrogen from the milling vessel was compensated by continuously feeding liquid nitrogen into the mill to guarantee complete immersion of the powders. The rotation speed was kept constant at 220 RPM and the powders were milled for 32 h. A powder-to-ball-weight ratio of 1:20 was used. The surface area of the powders after milling was measured using the BET technique.

High temperature oxidation tests of the cryomilled powders were conducted at three different temperatures: 500, 800, and 1,000 °C, respectively, for 48 h. The proposed temperatures cover different zones in the furnaces and boilers. Oxidation kinetics were measured using a gravimetric balance from Thermo Cahn. The apparatus continuously monitors the specimen's weight during testing with a recording microbalance. The powders were then put in a ceramic crucible, suspended from the microbalance by a preoxidized wire, and placed in a vertical tube furnace. The tube furnace was purged with argon, evacuated, and preheated at a heating rate of 10 °C per minute. Pure, dry flowing air was injected into the tube furnace and recordings of the weight changes were taken when the target temperature of the tube furnace was reached.

The milled powders and oxidation products were characterized by X-ray diffraction, scanning electron microscopy (SEM), transmission electron microscopy (TEM), and X-ray Photoelectron Spectrometer (XPS). Grain size measurement was carried out using CLEMEX image analysis software on TEM dark field micrographs.

Engineering the starting powders

The concentration of aluminum as the solute in the powders should be above the critical concentration necessary to establish a continuous protective layer of aluminum oxide during oxidation. The critical concentration of aluminum above which aluminum oxide is formed was calculated using the following equation [4]:

$$N_{\mathrm{Al}} = \frac{v}{z_{\mathrm{Al}} M_0} \times \left(\pi k_p / D\right)^{\frac{1}{2}} \quad (1)$$

In this equation v is the molar volume of the milled powder, Z_{Al} is the valence of the aluminum atoms, M_0 is the atomic weight of oxygen, D is the diffusion coefficient of aluminum in the iron and nickel [8, 9], and k_p is the rate constant for oxidation. Figure 1 presents the theoretical critical Al concentration in stainless steel powder and in Ni–20Cr–Al required to form the desired aluminum oxide scale as a function of temperature using the relationship presented in Eq. 1. The Al critical concentration curve presented represents the theoretical behavior of micro-sized grain material. The coefficient of diffusion of Al in conventional material was used to predict the curve as no values for the coefficient of diffusion of Al in nanostructured material were found in the literature. Nevertheless, the critical concentration curve of

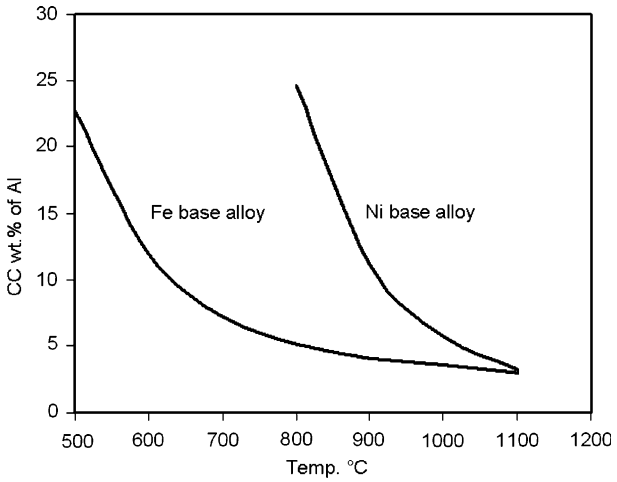

Fig. 1 Theoretical Al concentration required to form the protective Al_2O_3 scale in iron- and nickel-based alloys

Al in nanostructured powder is expected to shift down. Studies performed by Gao and Zhengwei [6] on an Al-containing nickel-based alloy (Ni–20Cr–Al) were verified using Eq. 1. At 1,000 °C, the critical concentration of aluminum required to form the Al_2O_3 protective layer was calculated to be 6 wt.%. Gao and Zhengwei showed experimentally that for an alloy containing 6 wt.% Al and possessing an average grain size of 10 μm, the aluminum oxide scale was developed. In addition, they verified that for the same alloy with an average grain size of 60 nm, only 2 wt.% of Al was necessary to develop the Al_2O_3 scale, which is three times lower than for the conventional materials. In this study, 6 wt.% Al in stainless steel was selected since the concentration is slightly above the critical concentration for the formation of aluminum oxide scale at 800 °C.

Results and discussions

The X-ray diffraction spectra of the cryomilled powders indicated that complete alloying of the Al was achieved after 32 h of milling. Examination by TEM of the cryomilled powders after 32 h reveals that the structure was in nanometer scale. A representative dark field micrograph and grain size distribution of the as-milled 316LSS-6 wt.% Al powders are presented in Fig. 2a and b. After examination of over 1,100 individual grains, the measured average grain size of the as-milled powders was 6.7 nm. The grain size distribution shows a narrow distribution, where most of the grains are smaller than 10 nm. Combination of the XRD and the TEM results reveals successful mechanical alloying and grain refinements of the mixture by cryomilling due to good balance between cold welding and fracturing processes of the powders. Similar grain refinement and alloying kinetics were described by Huang and Lavernia for the Fe-10 wt.% Al powder system. They also reported in their study that complete alloying was obtained after 25 h of milling and the final average grain size was 6 nm [10].

The oxidation kinetics results for the cryomilled powders tested for 48 h at 500, 800, and 1,000 °C, respectively, are presented in Fig. 3a and b, respectively. For comparison, conventional 316LSS powders were also tested. For all tested temperatures, the nanocrystalline 316LSS-6 wt.% Al powders showed a lower weight gain and better oxidation than the conventional 316LSS powders. At 500 and 800 °C the weight gain of the nanostructured powders was almost two times lower than that of the micron-sized powders, while the weight gain was seven times lower for the nanocrystalline 316LSS-6 wt.% Al at 1,000 °C.

The morphology of the different oxide scales and the respective qualitative compositions were studied using SEM. Figure 4a depicts the surface morphology of the oxide scale developed at the surface of conventional SS316L powders after a heat treatment of 48 h at 800 °C and Fig. 4b shows the corresponding EDS analysis of the surface. As expected, the surface is covered by a Cr_2O_3 layer. The EDS spectra show the presence of Fe, Si, Mn, and Ni, which are believe to come from the bulk of the particle since the interaction volume is larger than the thickness of the scale. Some well-defined crystals are observed and their analysis indicated Cr, Ni, and O, which would correspond to $NiCr_2O_4$ spinel crystals. Figure 4c shows the oxide grown on nanocrystalline powders containing 6 wt.%Al for the same heat treatment conditions and Fig. 4d presents the corresponding EDS analysis. It is worth mentioning that the EDS analyses were performed at 5 keV, to limit the interaction volume between the beam and the material. Monte Carlo simulation using Electron Flight Simulator software indicated that the interaction volume would penetrate 250 nm deep into the substrate. The results suggest that the oxide layer is composed of Al_2O_3 and the detection of Fe and Ni would be generated by the bulk. The absence of Cr toward the surface of the particles would confirm that the formation of a Cr-based oxide was prevented by the preferred development of the Al_2O_3 scale. A previous study has reported that during oxidation of nanoaluminum, the α-Al_2O_3 scale starts forming at 740 °C [11], and thus it is expected that α-Al_2O_3 will also be the grown oxide in the present work due to the faster nucleation of this stable reaction product.

To validate the EDS analysis, XPS analysis of the thermally grown oxides was carried out for the three tested temperatures. Figure 5 shows the oxygen 1s spectra for the samples tested at 500, 800, and 1,000 °C, respectively. For the scale formed at 500 °C, the O 1s reflection line of the

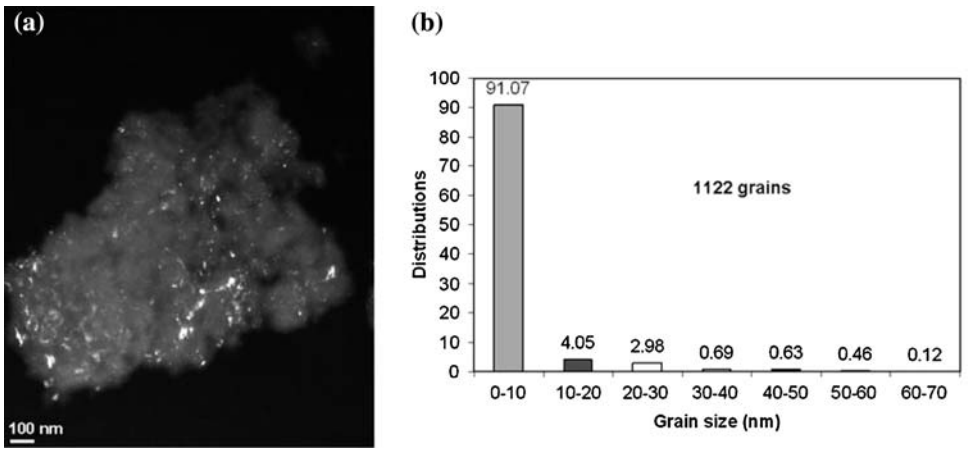

Fig. 2 (**a**) Dark field TEM micrograph of a nanostructured particle as-milled for 32 h and (**b**) grain size distribution measured from the TEM micrographs

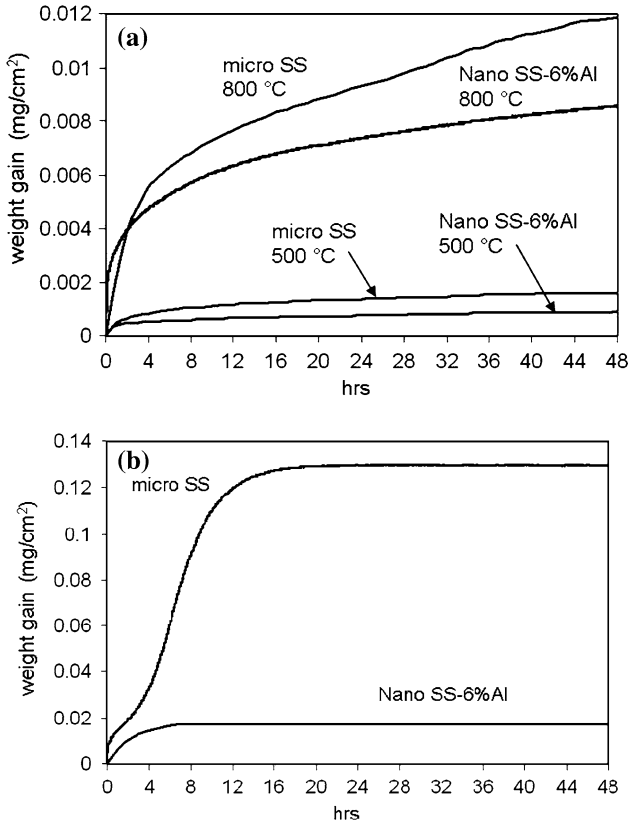

Fig. 3 Oxidation kinetic of micro-SS and nanostructured SS316-6 wt.%Al powders at (**a**) 500 and 800 °C and (**b**) 1,000 °C

surface oxide is located at 531.0 eV, which corresponds to the nominal value for Al_2O_3 [12]. With increasing oxidation temperature, the position of the O 1s peak slightly shifts toward lower energy. For the oxide scale grown at 800 °C, the reflection is observed at 530.2 eV, while the peaks for the oxide formed at 1,000 °C is located at 529.8 eV. This reduction in bonding energy is in agreement with the results published by Gewinner et al. [13], which showed a reduction of 1 eV in bonding energy between Al_2O_3 and Cr_2O_3 and the overall results correlate with the SEM observations.

Figure 6a shows a SEM micrograph of the cross section of polished 316LSS-6 wt.% Al particles oxidized for 48 h at 800 °C. As depicted in the surface oxide micrograph, most of the particles showed a completed outer Al_2O_3 scale, and a representative low voltage lines scan of this oxide scale is shown in Fig. 6b. In some cases, the thermally grown oxide scale possesses a Cr_2O_3 layer underneath the Al_2O_3 scale, which is caused by local depletion of Al. Upon formation of the initial Al_2O_3 oxide scale, the concentration of aluminum becomes lower than the critical concentration to sustain growth of the oxide, and nucleation of the second most favorable metal oxide begins. A representative low voltage line scan of this double oxide layer is shown in Fig. 6c. It is believed that for such low oxidation time (48 h), the premature depletion in aluminum is caused by a non-homogenous distribution of Al in the stainless steel powder after cryomilling.

Figure 7 presents a representative TEM dark field micrograph and grain size distribution of a milled particle heat treated at 500 °C for 120 h. Image analysis of the TEM micrographs yielded an average grain size of 11.4 nm after the heat treatment at 500 °C. The thermal stability shown by the powder is similar to other Al-containing iron powders manufactured by cryomilling. In fact, results from Witkin and Lavernia have shown that the thermal stability of al-containing iron powders remains in the nanometric grain size range up to 0.7*Mp of the alloy [7].

The results presented demonstrate that stainless steel containing ~6 wt.% Al can form the desired protective Al_2O_3 scale at 500 °C while maintaining an average grain size in the nanometer range. In comparison with the theoretical behavior of micron-sized grain SS (see Fig. 1), the major benefit in using an alloy containing Al resides in the development of an Al_2O_3 scale which was found several times more resistant to weight gain than the scale

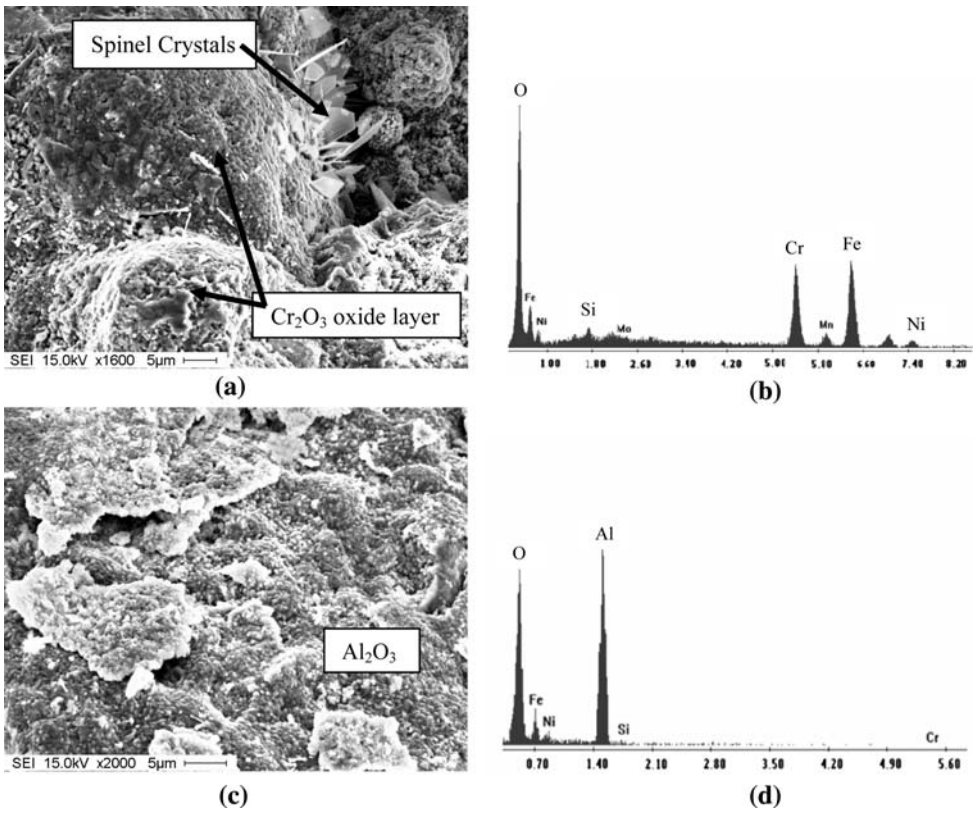

Fig. 4 (**a**) Secondary electron SEM image illustrating the oxide scale of conventional 316LSS and (**b**) the corresponding EDS analysis, (**c**) SEM micrograph of the surface of the oxide scale present on cryomilled SS 316-6 wt.%Al and (**d**) corresponding EDS analysis

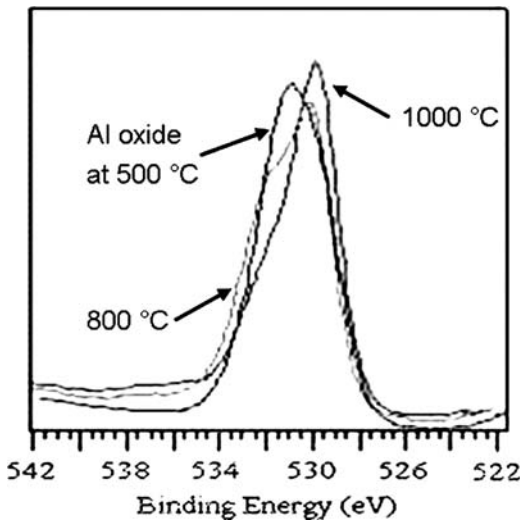

Fig. 5 XPS multiplex spectra for SS 316L-6 wt.% Al powder samples after heat treatment at 500, 800, and 1,000 °C, respectively

developed in conventional material. It is also worth mentioning that the formation of Al_2O_3 at the tested temperatures in a nanostructured material occurs at a lower Al concentration than for an Al-containing iron-based alloy with conventional grain size [14, 15]. This is attributed to short-circuit outward diffusion of aluminum through the grain boundaries. In addition, the good grain growth stability may originate from fine dispersed particles formed during cryomilling that subsequently impeded grain growth [16].

The activation energy from the oxidation reactions was calculated from the slope of the Arrhenius equation of oxidation rate constants (k_p) for conventional 316LSS and nanocrystalline 316LSS-6 wt.% Al powders, as shown in Fig. 8. The calculated activation energy for the oxidation reaction of the nanocrystalline powders was 85 kJ/mol, which is approximately half the calculated activation energy of conventional 316LSS (181 kJ/mol). A study of the oxidation of aluminum powders showed that the activation energy of the nano-sized powders was approximately 33% lower than the activation energy of the same powder in the micron-scale range [11]. The reduction of the activation energy can be explained by the increased volume fraction of the grain boundaries in nanostructured materials compared to the conventional materials. Grain boundaries are sites of fast diffusion paths for atoms (D_{gb}), which significantly enhance the overall effect of diffusion (D_{eff}) and can be calculated by Eq. 2 [17].

$$D_{\text{eff}} = gD_{gb} + (1-g)D_g \tag{2}$$

In the preceding equation D_g is the lattice diffusion and g is the volume fraction of the grain boundaries. Fast overall diffusion in nanocrystalline powders accelerates the oxidation process which lowers the Al concentration needed to form healing oxide scale as was observed at 500 °C.

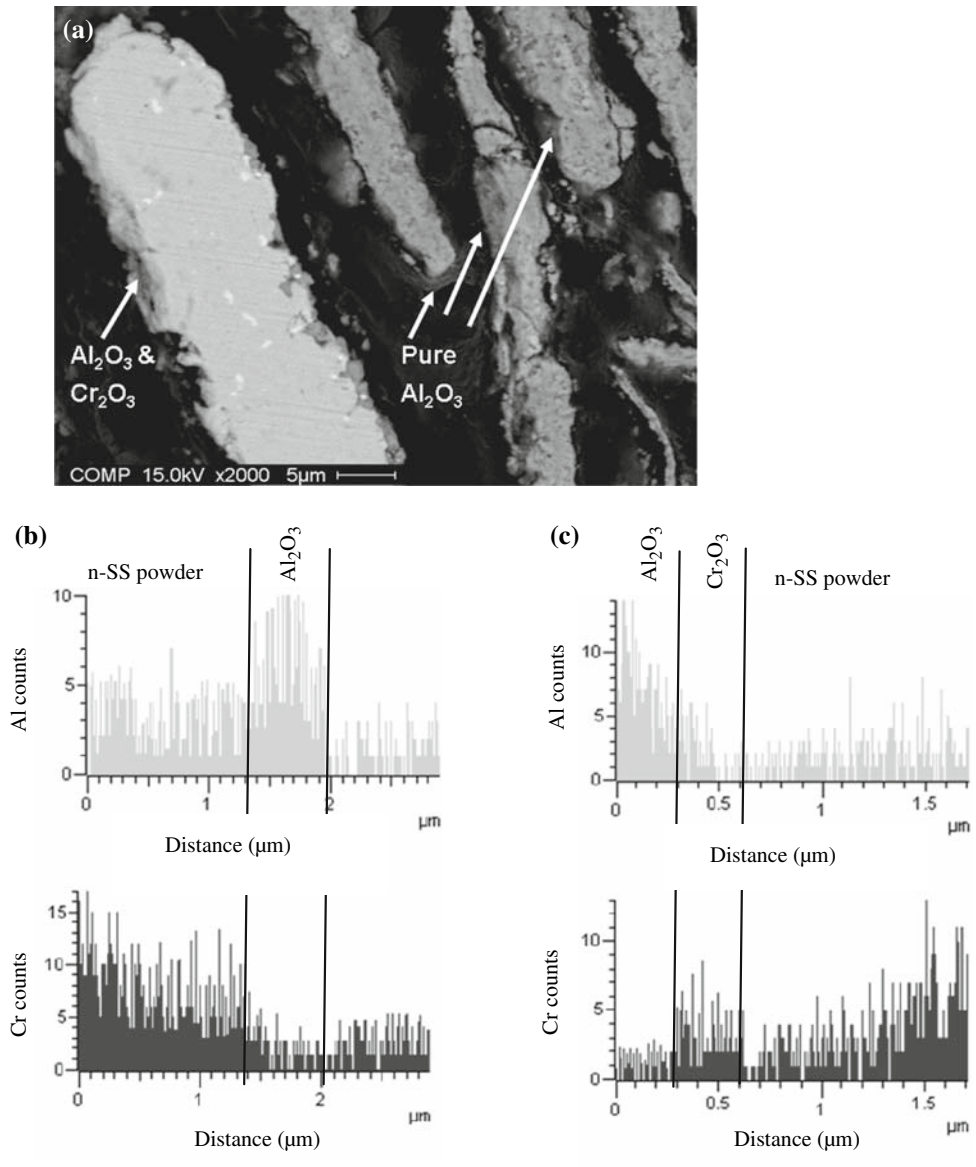

Fig. 6 (**a**) SEM micrograph of the cross-section of nanostructured powders oxidized at 800 °C for 48 h, and (**b**) and (**c**) low voltage line scans of the single and double layer oxide scale

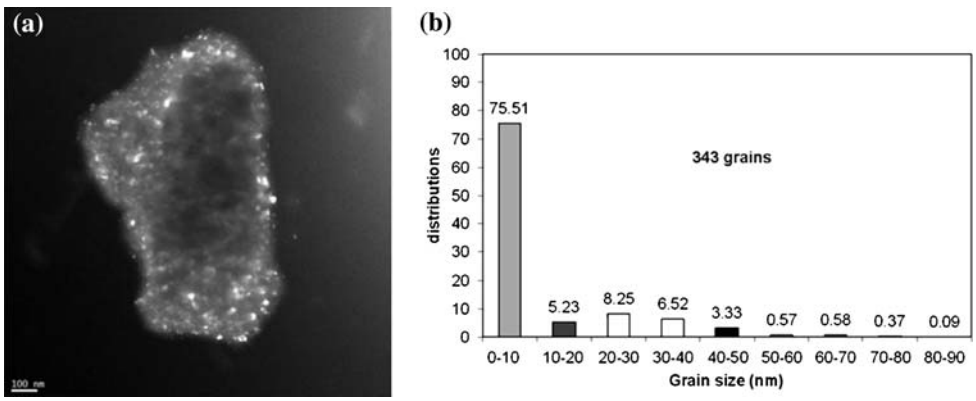

Fig. 7 (**a**) Dark field TEM micrograph of a nanostructured particle heat treated at 500 °C for 120 h. (**b**) Grain size distribution of the TEM image

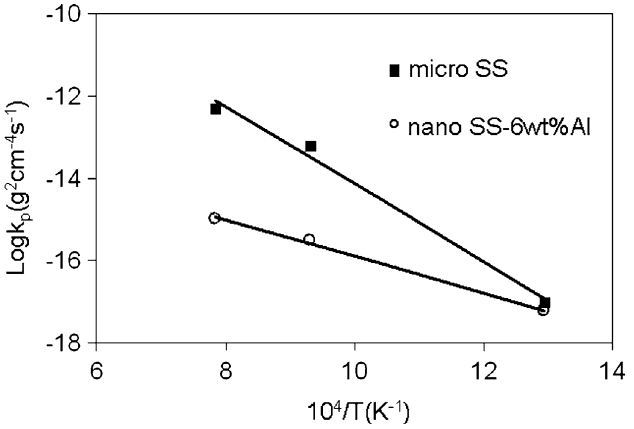

Fig. 8 Arrhenius plot of the parabolic oxidation of micro-SS and nano SS-6 wt.%Al

Conclusions

Nanocrystalline 316LSS containing 6 wt.% Al was successfully produced by cryomilling. The cryomilled powder demonstrated good grain growth stability at 500 °C when the powders had been heat treated for 120 h, and the average grain size was found to be 11.4 nm. The XPS and SEM/EDS analyses showed that pure aluminum oxide scale formed and was the predominant oxide phase after heat treatment at 500 °C. The activation energy of the nanostructured powders was found to be almost 50% lower (85 vs. 181 kJ/mol) than the conventional powders due the higher number of grain boundaries, which resulted in a higher rate of diffusion in the nanostructured powders.

Acknowledgements The authors would like to acknowledge Saudi Aramco Company, which generously awarded financial support to A. Almathami. The authors would also like to thank McGill University and Hoganas for providing the starting powders.

References

1. Uunsitalo M et al (2003) Mater Sci Eng A346:168
2. Quadakkers W et al (1998) In: Proceeding of the International Conference of Corrosion. Elsevier, Amsterdam, Mumbai, India, December 1997, p 199
3. Ramakrishnan V (1988) Oxid Met 30:185
4. Wood G (1970) Oxid Met 2:11
5. Stott F, Wei F (1989) Oxid Met 31:369
6. Gao W, Zhengwei L (2004) Mat Res 7:175
7. Witkin D, Lavernia E (2006) Prog Mater Sci 51:1
8. Gemmaz M et al (1990) Surf Sci Lett 227:L109
9. Nakamura R et al (2002) Intermetallics 10:195
10. Huang B, Lavernia E (1998) Mater Sci Eng A255:124
11. Pivkna A et al (2004) J Mater Sci 39:5451
12. Handbook of X-ray Photoelectron Spectroscopy (1992) Perkin-Elmer Corporation, p 44
13. Gewinner G et al (1978) Surf Sci 78:439
14. Jun-huai X et al (2006) Trans Nonferr Met Soc China 16:s829
15. Dunning J et al (2002) Oxid Met 57:409
16. Perez R, et al (1996) NanoStruct Mater 7:565
17. Hart EW (1957) Acta Metall 5:597